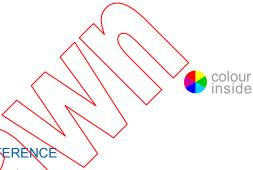


# **CISPR/TR 16-3**

Edition 3.0 2010-08

# TECHNICAL REPORT



INTERNATIONAL SPECIAL COMMITTEE ON RADIO INTERFERENCE

Specification for radio disturbance and immunity measuring apparatus and methods –

Part 3: CISPR technical reports



INTERNATIONAL ELECTROTECHNICAL COMMISSION

PRICE CODE

ICS 33.100.10; 33.100.20 ISBN 978-2-88912-147-2

# **CONTENTS**

FO	REW	ORD		14
1	Scop	ре		16
2	Norn	native re	eferences	16
3	Term	ns. defin	nitions and abbreviations	17
	3.1		and definitions	
	3.2		viations	
4			ports	
•	4.1	Correl charac	ation between measurements made with apparatus having cteristics differing from CISPR characteristics and measurements made	20
		4.1.1	General	_
		4.1.2	Critical interference-measuring instrument parameters	
		4.1.3	Impulse interference – correlation factors	23
		4.1.4	Random noise	25
		4.1.5	The root mean square (rms) detector.	25
		4.1.6	Discussion	25
		4.1.7	Application to typical noise sources	25
		4.1.8	Conclusions	
	4.2	Interfe	erence simulators	27
		4.2.1	General	27
		4.2.2	Types of interference signals	27
		4.2.3	Circuits for simulating broadband interference	28
	4.3		onship between limits for open-area test site and the reverberation	
		chamb		
		4.3.1	General	32
		4.3.2	Correlation between measurement results of the reverberation chamber and QATS	
		4.3.3	Limits for use with the reverberation chamber method	33
		4.3.4	Procedure for the determination of the reverberation chamber limit	33
	4.4 Characterization and classification of the asymmetrical disturbance so induced in telephone subscriber lines by AM broadcasting transmitters the LW. MW and SW bands			
		4.4.1	General	34
		4.4.2	Experimental characterization	
		4.4.3	Prediction models and classification	
		4.4.4	Characterization of the immunity-test disturbance source	
	4.5		stability of radiation in vertical directions at frequencies above 30 MHz	
	4.5	4.5.1	Summary	
		4.5.2	Range of application	
		4.5.3	General	
		4.5.4	Method used to calculate field patterns in the vertical plane	
		4.5.5	Limitations of predictability of radiation at elevated angles	
		4.5.6	Differences between the fields over a real ground and the fields over	55
		∓. <b>U</b> .U	a perfect conductor	87
		4.5.7	Uncertainty ranges	
		4.5.8	Conclusions	

5

4.6	The pr	edictability of radiation in vertical directions at frequencies up to	97
	4.6.1	Range of application	
	4.6.2	General	
	4.6.3	Method of calculation of the vertical radiation patterns	
	4.6.4	The source models	
	4.6.5	Electrical constants of the ground	
	4.6.6	Predictability of radiation in vertical directions	
	4.6.7	Conclusions	
	4.6.8	Figures associated with predictability of radiation in vertical directions	
4.7	Correl of dist	ation between amplitude probability distribution (APD) characteristics urbance and performance of digital communication systems	139
	4.7.1	General	139
	4.7.2	Influence on a wireless LAN system	139
	4.7.3	Influence on a Bluetooth system	142
	4.7.4	Influence on a W-CDMA system	146
	4.7.5	Influence on Personal Handy Phone System (PHS)	149
	4.7.6	Quantitative correlation between noise parameters and system performance	153
	4.7.7	Quantitative correlation between noise parameters of repetition pulse and system performance of RHS and W-CDMA (BER)	157
4.8	_	round material on the definition of the rms-average weighting detector	
		asuring receivers	
	4.8.1	General purpose of weighted measurement of disturbance	
	4.8.2	General principle of weighting the CISPR quasi-peak detector	
	4.8.3	Other detectors defined in CISPR 16-1-1	161
	4.8.4	Procedures for measuring pulse weighting characteristics of digital radiocommunications services	
	4.8.5	Theoretical studies	
	4.8.6	Experimental results	167
	4.8.7	Effects of spread-spectrum clock interference on wideband radiocommunication signal reception	185
	4.8.8	Analysis of the various weighting characteristics and proposal of a	
<		weighting detector	
	4.8.9	Properties of the rms-average weighting detector	
4.9		on mode absorption devices (CMAD)	
	4.9.1	General	
	4.9.2	CMAD as a two-port device	
	4.9.3	Measurement of CMAD	
4.10	_	round on the definition of the FFT-based receiver	
		General	
		Tuned selective voltmeters and spectrum analyzers	
		General principle of a tuned selective voltmeter	
		FFT-based receivers – digital signal processing	
	4.10.5	Measurement errors specific to FFT processing	213
		FFT-based receivers – examples	
Back	kground	and history of CISPR	228
5.1	The hi	story of CISPR	228
	5.1.1	The early years: 1934-1984	228

	5.1.2	The	division of	work					230
	5.1.3	The	computer y	ears: 1984	to 1998				230
	5.1.4	The	people in C	ISPR					231
5.2				o the metho ctrical hous					
	_								231
	5.2.1								
Λ Α	5.2.2		•	the method					232
									234
	•	•		•	•		. (	bution	
	•	•		-voltage dis			^		245
	•	,		hematical r				//	247
				fields radia			s from 27	MHz ISM	249
Bibliogra	phy							·	255
							1/		
Figure 1	– Relati	ve res	sponse of v	arious dete	ctors to im	pulse inte	rference		22
Figure 2	– Pulse	rectif	ication coe	fficient $P(\alpha)$		<u>}</u> /\			23
Figure 3	– Pulse	repet	ition freque	ency			<u> </u>		24
Figure 4	– Block	diagr	am and wa	veforms of	a simulator	generatir	ng noise bu	ırsts	30
_	– Block	diagr	am of a sim			/-	according t	to the pulse	
•				nut etaga		<b>v</b>			
				put stage Isured outd	. 1				52
versus th	e calcul	ated	outdoor ma	gnetic field	strength H	c dB(μA/r	n)		36
Figure 8 effect par			outdoor mag	gnetic versi	is distance	, and prob	pability of t	he building-	37
Figure 9	– Norma	a pro	bability plot	of the build	ding-effect	paramete	r A <sub>b</sub> dB		38
Figure 10 antenna 1	- Scat	ter plo	ot of the ou	tdoor anten	na factor G	$G_0$ dB( $\Omega$ m	) versus th	e indoor	39
	/ \	· 👠	• \						
Figure 12	2 – Norn	nal pr	obability plo	ot of the eq	uivalent as	ymmetrica	al resistan		
<b>-</b>		~							
•		•		• •		•			
								······································	49
maximum	n field st	rengt	h $E_{O}$ resulti	e. the distr ng from a g n	given numb	er of trans	smitters in		50
Figure 16	S – Exan	nple c	of the numb	er of outlets	s with an in	iduced as	ymmetrica		
Figure 17	′ – Exan	nples	of number	(left-hand s	scale) and r	elative nu	ımber (righ		
Figure 18	3 – Verti	cal po	olar pattern	s of horizor	ntally polari	zed $E_x$ fie	ld strength		
									61
				of vertically				itted from real ground	61

Figure 20 – Vertical polar patterns of horizontally polarized $E_\chi$ field strengths emitted around small vertical loop (horizontal magnetic dipole), over three different types of real ground
Figure 21 – Vertical polar patterns of vertically oriented $E_z$ field strengths emitted around small vertical loop (horizontal magnetic dipole) over three different types of real ground
Figure 22 – Height scan patterns of vertically oriented $E_z$ field strengths emitted at 1 000 MHz from the small vertical loop (horizontal magnetic dipole), at horizontal distance of 10 m, 30 m and 300 m in the Z-X plane over three different types of real ground
Figure 23 – Vertical polar patterns of horizontally polarized $E_{\chi}$ and vertically oriented $E_{Z}$ field strengths emitted around small horizontal electric dipole, in Y-Z and Z-X planes respectively
Figure 24 – Height scan patterns of horizontally polarized $E_{\chi}$ field strengths emitted from small horizontal electric dipole
Figure 25 – Vertical polar patterns of horizontally polarized $E_x$ and vertically oriented $E_z$ field strengths emitted around small horizontal electric dipole in Y-Z and Z-X planes respectively
Figure 26 – Height scan patterns of horizontally polarized E <sub>x</sub> field strengths emitted small horizontal electric dipole
Figure 27 – Vertical polar patterns of horizontally polarized $E_{\rm x}$ and vertically oriented $E_{\rm z}$ field strengths emitted around small vertical toop (horizontal magnetic dipole) in Y-Z and Z-X planes respectively
Figure 28 – Height scan patterns of vertically oriented $E_x$ and horizontally oriented $E_x$ field strengths emitted from small vertical loop (horizontal magnetic dipole)70
Figure 29 – Vertical polar patterns of vertically oriented $E_z$ and horizontally oriented $E_x$ field strengths emitted around small vertical electric dipole73
Figure 30 – Height scan patterns of vertically oriented $E_z$ and horizontally oriented $E_x$ field strengths emitted from small vertical electric dipole73
Figure 31 – Vertical polar patterns of horizontally polarized $E_X$ and vertically oriented $E_Z$ field strengths emitted around small vertical loop (horizontal magnetic dipole) in Y-Z and Z-X planes respectively74
Figure 32 – Height scan patterns of vertically oriented $E_z$ and horizontally oriented $E_\chi$ field strengths emitted from small vertical loop (horizontal magnetic dipole)74
Figure 33 – Vertical polar patterns of horizontally polarized <i>E</i> -field strength emitted around small horizontal loop (vertical magnetic dipole)
Figure 34 – Height scan patterns of horizontally polarized $E$ -field strength emitted from small horizontal loop (vertical magnetic dipole)75
Figure 35 – Vertical polar patterns of vertically oriented $E_z$ and horizontally oriented $E_\chi$ field strengths emitted around small vertical electric dipole
Figure 36 – Height scan patterns of vertically oriented $E_z$ and horizontally oriented $E_\chi$ field strengths emitted from the small vertical electric dipole
Figure 37 – Vertical polar patterns of horizontally polarized $E_{\chi}$ and vertically oriented $E_{Z}$ field strengths emitted around small vertical loop (horizontal magnetic dipole) in Y-Z and Z-X planes respectively79
Figure 38 – Height scan patterns of vertically oriented $E_z$ and horizontally oriented $E_\chi$ field strengths emitted from small vertical loop (horizontal magnetic dipole)79
Figure 39 – Vertical polar patterns of horizontally polarized <i>E</i> -field strength emitted around small horizontal loop (vertical magnetic dipole)80
Figure 40 – Height scan patterns of horizontally polarized <i>E</i> -field strength emitted from small horizontal loop (vertical magnetic dipole)80

Figure 41 – Vertical polar patterns of horizontally polarized <i>E</i> -field strength emitted around the small horizontal loop (vertical magnetic dipole)	83
Figure 42 – Height scan patterns of horizontally polarized <i>E</i> -field strength emitted from small horizontal loop (vertical magnetic dipole)	83
Figure 43 – Height scan patterns of horizontally polarized <i>E</i> -field strength emitted from small horizontal loop (vertical magnetic dipole)	87
Figure 44 – Height scan patterns of the vertical component of the <i>E</i> -fields emitted from a small vertical electric dipole	90
Figure 45 $-$ Height scan patterns of the vertical component of the $\it E$ -fields emitted from a small vertical electric dipole	90
Figure 46 – Height scan patterns of the horizontally polarized <i>E</i> -fields emitted in the vertical plane normal to the axis of a small horizontal electric dipole	92
Figure 47 – Height scan patterns of the horizontally polarized <i>E</i> -fields emitted in the vertical plane normal to the axis of a small horizontal electric dipole	92
Figure 48 – Ranges of uncertainties in the predictability of radiation in vertical directions from electrically small sources located at a height of 1 m or 2 m above	04
Figure 49 – Ranges of uncertainties in the predictability of radiation in vertical	94
directions from electrically small sources located at a height of 1 m or 2 m above ground	95
Figure 50 – Ranges of uncertainties in the predictability of radiation in vertical directions from electrically small sources located at a height of 1 m or 2 m above ground	96
Figure 51 – Geometry of the small vertical electric dipole model	100
Figure 52 – Geometry of the small horizontal electrical dipole model	
Figure 53 – Geometry of the small horizontal magnetic dipole model (small vertical loop)	100
Figure 54 – Geometry of the small vertical magnetic dipole model (small horizontal loop)	100
Figure 55 – Ranges of errors in the predictability of radiation in vertical directions from electrically small sources located close to the ground, based on measurements of the horizontally oriented <i>H</i> -field near ground at a distance of 30 m from the sources	108
Figure 56 – Ranges of errors in the predictability of radiation in vertical directions from electrically small sources located close to the ground, based on measurements of the horizontally oriented <i>H</i> -field at the ground supplemented with measurements of the vertically oriented <i>H</i> -field in a height scan up to 6 m at a distance of 30 m from the	
sources	109
Figure 57 – Vertical radiation patterns of horizontally oriented <i>H</i> -fields emitted by a small vertical electric dipole located close to the ground	111
Figure 58 – Vertical radiation patterns of horizontally oriented <i>H</i> -fields emitted by a small vertical electric dipole located close to the ground	111
Figure 59 – Vertical radiation patterns of <i>E</i> -fields emitted by a small vertical electric dipole located close to the ground	112
Figure 60 $-$ Vertical radiation patterns of the $\it E$ -fields emitted by a small vertical electric dipole located close to the ground	112
Figure 61 – Vertical radiation patterns of the <i>H</i> -fields emitted by a small horizontal electric dipole located close to the ground	113
Figure 62 – Influence of a wide range of values of the electrical constants of the ground on the vertical radiation patterns of the horizontally oriented $H$ -fields emitted by a small horizontal electric dipole located close to the ground	113
Figure 63 – Vertical radiation patterns of the horizontally oriented <i>H</i> -fields emitted by a small horizontal electric dipole located close to the ground	114

Figure 64 – Vertical radiation patterns of the <i>E</i> -fields emitted by a small horizontal electric dipole located close to the ground	114
Figure 65 – Vertical radiation patterns of the <i>E</i> -fields emitted by a small horizontal electric dipole located close to the ground	115
Figure 66 – Vertical radiation patterns of <i>H</i> -fields emitted by small horizontal magnetic dipole (vertical loop) located close to ground	115
Figure 67 – Vertical radiation patterns of the horizontally oriented <i>H</i> -fields emitted by a small horizontal magnetic dipole (vertical loop) located close to the ground	116
Figure 68 – Vertical radiation patterns of the horizontally oriented <i>H</i> -fields emitted by a small horizontal magnetic dipole (vertical loop) located close to the ground	116
Figure 69 – Vertical radiation patterns of the <i>E</i> -fields emitted by a small horizontal magnetic dipole (vertical loop) located close to the ground	117
Figure 70 – Vertical radiation patterns of the <i>E</i> -fields emitted by a small horizontal magnetic dipole (vertical loop) located close to the ground	117
Figure 71 – Vertical radiation patterns of the <i>H</i> -fields emitted by a small vertical magnetic dipole (horizontal loop) located close to the ground	118
Figure 72 – Vertical radiation patterns of the <i>H</i> -fields emitted by a small vertical magnetic dipole (horizontal loop) located close to the ground	118
Figure 73 – Vertical radiation patterns of the H-fields emitted by a small vertical	119
Figure 74 – Vertical radiation patterns of the H-fields emitted by a small vertical magnetic dipole (horizontal loop) located close to the ground	119
Figure 75 – Vertical radiation pattern of the <i>E</i> -field emitted by a small vertical magnetic dipole (horizontal loop) located close to the ground	120
Figure 76 – Vertical radiation patterns of the <i>E</i> -fields emitted by a small vertical magnetic dipole (horizontal loop) located close to the ground	120
Figure 77 – Vertical radiation patterns of the horizontally oriented H-fields emitted by a	121
Figure 78 – Vertical radiation patterns of the $E$ -fields emitted by a small vertical electric	121
Figure 79 – Vertical radiation patterns of the $E$ -fields emitted by a small vertical electric	122
Figure 80 – Vertical radiation patterns of the <i>H</i> -fields emitted by a small horizontal electric globe located close to the ground	122
Figure 81 – Vertical radiation patterns of the horizontally oriented <i>H</i> -fields emitted by a small horizontal electric dipole located close to the ground	
Figure 82 – Vertical radiation patterns of the <i>E</i> -fields emitted by a small horizontal electric dipole located close to the ground	
Figure 83 – Vertical radiation patterns of the <i>E</i> -fields emitted by a small horizontal electric dipole located close to the ground	
Figure 84 – Vertical radiation patterns of the <i>H</i> -fields emitted by a small horizontal magnetic dipole (vertical loop) located close to the ground	
Figure 85 – Vertical radiation patterns of the horizontally oriented <i>H</i> -fields emitted by a small horizontal magnetic dipole (vertical loop) located close to the ground	
Figure 86 – Vertical radiation patterns of the horizontally oriented <i>H</i> -fields emitted by a small horizontal magnetic dipole (vertical loop) located close to the ground	
Figure 87 – Vertical radiation patterns of the <i>E</i> -fields emitted by a small horizontal magnetic dipole (vertical loop) located close to the ground	
Figure 88 – Vertical radiation patterns of the <i>E</i> -fields emitted by a small horizontal magnetic dipole (vertical loop) located close to the ground	

Figure 89 – Vertical radiation patterns of the <i>H</i> -fields emitted by a small vertical magnetic dipole (horizontal loop) located close to the ground	. 127
Figure 90 – Vertical radiation patterns of the <i>H</i> -fields emitted by a small vertical magnetic dipole (horizontal loop) located close to the ground	. 127
Figure 91 – Vertical radiation patterns of the <i>H</i> -fields emitted by a small vertical magnetic dipole (horizontal loop) located close to the ground	. 128
Figure 92 – Vertical radiation patterns of the <i>E</i> -fields emitted by a small vertical magnetic dipole (horizontal loop) located close to the ground	. 128
Figure 93 – Vertical radiation patterns of the horizontally oriented $H$ -fields emitted by a small vertical electric dipole located close to the ground	. 129
Figure 94 – Vertical radiation patterns of the <i>E</i> -fields emitted by a small vertical electric dipole located close to the ground	. 129
Figure 95 – Vertical radiation patterns of the <i>E</i> -fields emitted by a small vertical electric dipole located close to the ground	. 130
Figure 96 – Vertical radiation patterns of the <i>H</i> -fields emitted by a small horizontal electric dipole located close to the ground	. 130
Figure 97 – Vertical radiation patterns of the <i>E</i> -fields emitted by a small horizontal electric dipole located close to the ground	. 131
Figure 98 – Vertical radiation patterns of the <i>E</i> -fields emitted by a small horizontal electric dipole located close to the ground	. 131
Figure 99 – Vertical radiation patterns of the H-field emitted by a small horizontal magnetic dipole (vertical loop) located close to the ground	. 132
Figure 100 – Vertical radiation patterns of the vertically polarized <i>E</i> -fields emitted by a small horizontal magnetic dipole (vertical loop) located close to the ground	. 132
Figure 101 – Vertical radiation patterns of the Hyfield emitted by a small vertical magnetic dipole (horizontal loop) located close to the ground	. 133
Figure 102 – Vertical radiation patterns of the E-fields emitted by a small vertical magnetic dipole (horizontal loop) located close to the ground	. 133
Figure 103 – Vertical radiation patterns of the horizontally oriented $H$ -fields emitted by a small vertical electric dipole located close to the ground	. 134
Figure 104 – Vertical radiation patterns of the vertically polarized <i>E</i> -fields emitted by a small vertical electric dipole located close to the ground	. 134
Figure 105 – Vertical radiation patterns of the <i>H</i> -fields emitted by a small horizontal electric dipole located close to the ground	. 135
Figure 106 - Vertical radiation patterns of the horizontally oriented $H$ -fields emitted by a small horizontal electric dipole located close to the ground	. 135
Figure 107 – Influence of a wide range of values of the electrical constants of the ground on the vertical radiation patterns of the horizontally oriented <i>H</i> -fields emitted by a small horizontal electric dipole located close to the ground	. 136
Figure 108 – Vertical radiation patterns of the vertically polarized <i>E</i> -fields emitted by a small horizontal electric dipole located close to the ground	. 136
Figure 109 – Vertical radiation patterns of the $H$ -fields emitted by a small horizontal magnetic dipole (vertical loop) located close to the ground	. 137
Figure 110 – Vertical radiation patterns of the vertically polarized <i>E</i> -fields emitted by a small horizontal magnetic dipole (vertical loop) located close to the ground	. 137
Figure 111 – Vertical radiation patterns of the $H$ -fields emitted by a small vertical magnetic dipole (horizontal loop) located close to the ground	. 138
Figure 112 – Vertical radiation patterns of the <i>E</i> -fields emitted by a small vertical magnetic dipole (horizontal loop) located close to the ground	. 138
Figure 113 – Set-up for measuring communication quality degradation of a wireless LAN	. 139

Figure 114 – APD characteristics of disturbance	141
Figure 115 – Wireless LAN throughput influenced by noise	142
Figure 116 – Set-up for measuring the communication quality degradation of Bluetooth	143
Figure 117 – APD of disturbance of actual MWO (2 441MHz)	143
Figure 118 – APD characteristics of disturbance (2 460 MHz)	144
Figure 119 – Throughput of Bluetooth influenced by noise	146
Figure 120 – Set-up for measuring the BER of W-CDMA	147
Figure 121 – APD characteristics of disturbance	148
Figure 122 – BER of W-CDMA caused by radiation noise	149
Figure 123 – Set-up for measuring the PHS throughput	150
Figure 124 – Set-up for measuring the BER of PHS	150
Figure 125 – APD characteristics of disturbance	151
Figure 126 – PHS throughput caused by radiation	152
Figure 127 – BER of PHS caused by radiation noise	153
Figure 128 – Correlation of the disturbance voltages with the system performance $(C/N_0)$	154
Figure 129 – Correlation of the disturbance voltages with the system performance	155
Figure 130 - Correlation of the disturbance voltages with the system performance	155
Figure 131 – Correlation of the disturbance voltages with the system performance $(C/N_0)$	156
Figure 132 – Correlation of the disturbance voltages with the system performance $(C/N_0)$	156
Figure 133 – Experimental set-up for measuring communication quality degradation of a PHS or W-CDMA	157
Figure 134 – Simulation set-up for estimating communication quality degradation of a PHS or W-CDMA	157
Figure 135 – APD of pulse disturbance	158
Figure 136 – BER degradation of PHS and W-CDMA caused by repetition pulse (Carrier power –35 dBm)	158
Figure 137 – Evaluation method of the correlation between BER and APD	159
Figure 138 – Correlation between measured $\Delta$ $L_{\sf BER}$ and $\Delta$ $L_{\sf APD}$	
Figure 139 – Correlation between measured $p_{\sf BER}$ and $p_{\sf APD}$	
Figure 140 – Weighting curves of quasi-peak measuring receivers for the different frequency ranges as defined in CISPR 16-1-1	
Figure 141 – Weighting curves for peak, quasi-peak, rms and linear average detectors for CISPR bands C and D	162
Figure 142 – Test setup for the measurement of the pulse weighting characteristics of a digital radiocommunication system	163
Figure 143 – Example of an interference spectrum: pulse modulated carrier with a pulse duration of 0,2 μs and a PRF < 10 kHz	164
Figure 144 – The rms and peak levels for constant BEP for three $K = 3$ , convolutional codes of different rate	166
Figure 145 – The rms and peak levels for constant BEP for two rate ½, convolutional code	167
Figure 146 – Test setup for the measurement of weighting curves for Digital Radio Mondiale (DRM)	169

Figure 147 – Weighting characteristics for DRM signals for various pulse widths of the pulse-modulated carrier	170
Figure 148 – Weighting characteristics for DRM protection level 0: average of results for two receivers	171
Figure 149 – Weighting characteristics for DRM protection level 1: average of results for two receivers	171
Figure 150 – Weighting characteristics for DVB-T with 64 QAM 2k, <i>CR</i> 3/4 (as used in France and UK)	173
Figure 151 – Weighting characteristics for DVB-T with 64 QAM 8k, <i>CR</i> 3/4 (as used in Spain)	174
Figure 152 – Weighting characteristics for DVB-T with 16 QAM 8k, CR 2/3 (as used in Germany)	174
Figure 153 – Average weighting characteristics of 6 receiver types for DVB-T with 16QAM	175
Figure 154 – Average weighting characteristics of 6 receiver types for DVB-T with	176
Figure 155 – Weighting characteristics for DAB (signal level -71 dBm) with a tlat response down to approximately 1 kHz	177
Figure 156 – Weighting characteristics for DAB: average of two different commercial receiver types	177
Figure 157 – Weighting characteristics for TETRA (signal level – 80 dBm) for a code rate of 1	178
Figure 158 – Weighting characteristics for RBER 16 of GSM (signal level –90 dBm)	179
Figure 159 – Weighting characteristics for RBER 2 of GSM	179
Figure 160 – Carrier-to-interference improvements with decreasing PRF in dB computed for GSM using CQSSAP	180
Figure 161 – Rms and quasi peak values of pulse level for constant effect on FM radio reception	180
Figure 162 – Weighting characteristics for RBER 1b of GSM (signal level –90 dBm)	181
Figure 163 – Weighting characteristics for DECT (signal level –83 dBm)	182
Figure 164 – Weighting characteristics for IS-95 (signal level -97 dBm) with comparatively high immunity to interference	183
Figure 165 - Weighting characteristics for J-STD 008 (signal level –97 dBm)	
Figure 166 - Weighting characteristics for the Frame Error Ratio (FER) of CDMA2000 (measured at a receive signal level of –112 dBm) for a low data rate of 9,6 kb/s	
Figure 167 – Weighting characteristics for the Frame Error Ratio (FER) of CDMA2000 (measured at a receive signal level of –106 dBm) for two different data rates (9,6 kb/s	
and 76,8 kb/s)	185
Figure 168 – The proposed rms-average detector for CISPR Bands C and D with a corner frequency of 100 Hz	188
Figure 169 – Rms-average detector function by using an rms detector followed by a linear average detector and peak reading	188
Figure 170 – Rms-average weighting functions for CISPR Bands A, B, C/D and E for the shortest pulse widths allowed by the measurement bandwidths	189
Figure 171 – Shift of the rms-average weighting function for CISPR band C/D by using a bandwidth of 1 MHz instead of 120 kHz, if the shortest possible pulse widths are	
applied	
Figure 172 – Example of a simple EUT model	
Figure 173 – Representation of a CMAD as a two-port device	194

Figure 174 – Conformal mapping between <i>z</i> -plane and <i>f</i> -plane	196
Figure 175 – Conversion from 50 $\Omega$ coaxial system to the geometry of the two-port	100
device-under-test	198 199
Figure 177 – The four calibration configurations necessary for the TRL calibration	
Figure 178 – Measurement of CMAD characteristics	200
Figure 179 – Preliminary measurements of the test set-up	204
Figure 180 – Position of the reference planes for the measurement with SOLT	200
calibration and $ABCD$ transformation to $Z_{ref}$ level	207
Figure 181 – Superheterodyne EMI receiver	209
Figure 182 – An example spectrogram $Z[m,k]$	211
Figure 183 – Sidelobe effect due to the finite length of window	213
Figure 184 – Measurement error for a single pulse	214
Figure 185 – IF signal for different overlapping factors for the same sequence of	045
pulses.	215
Figure 186 – FFT-based baseband system	216
Figure 187 – Real-time FFT-based measuring instrument	217
Figure 188 – Digital down-converter.	217
Figure 189 – Short time fast Fourier transform – An example of implementation	218
Figure 190 – Floating-point analogue-to-digital conversion	218
Figure 191 – Example of a 120 kHz Gaussian filter	
Figure 192 – Essential parts of an EFT-based heterodyne receiver	220
Figure 193 – Dynamic range for broadband emission as measured with the peak detector	222
Figure 194 – Set-up of FFT-based system type 2	222
Figure 195 – FFT Software ("FFTemi") screen shot	225
Figure 196 – Example of pulse generator measurement with antenna	226
Figure 197 – Radiated emission measurement of a motor – peak detector	
Figure 198 – Angular characterization of a PC	227
Figure 199 Example FFT IF analysis display	
Figure A.1 Example plot using the expression $P_t + G = P_q + 2$	
Figure A.2 – Examples of a number of microwaves measured for $P_q$ and $P_t$	237
Figure B.1 – Definition of the ring-shaped area round the transmitter T	
Figure C.1 – The permissible ranges of $U_{\rm h}$ and $G$ are within the polygon $\{G_{\rm L}, U_{\rm a}\}$ , $\{G_{\rm L}, U_{\rm b}\}$ , $\{G_{\rm L}, U_{\rm d}\}$ , $\{G_{\rm L}, U_{\rm c}\}$ and $\{G_{\rm L}, U_{\rm a}\}$ . For the given value $U_{\rm L}$ the double-shaded area represents $pr\{U_{\rm h} \geq U_{\rm L}\}$	
Figure F.1 – Vertical radiation patterns of horizontally polarized fields, 109 MHz, 300 m	243
scan radius (adapted from [34])	251
Figure F.2 – Vertical radiation patterns of horizontally polarized fields, 109 MHz, 300 m scan radius (adapted from [34])	252
Figure F.3 – Vertical radiation patterns of horizontally polarized fields, 109 MHz, 300 m scan radius (adapted from [34])	253
Figure F.4 – Vertical radiation patterns of horizontally polarized fields, 109 MHz, 300 m scan radius (adapted from [34])	254

Table 1 – Comparative response of slideback peak, quasi-peak and average detectors to sine wave, periodic pulse and Gaussian waveform	22
Table 2 – Characteristics of gate generator and modulator to simulate various types of broadband interference	28
Table 3 – Summary results of building-effect, A <sub>b</sub> , analysis	38
Table 4 – Summary of results of <i>G</i> -factor analysis	41
Table 5 – Summary of $L_0$ factors (far-field)	41
Table 6 – Summary of truncation parameters of $f(G)$	
Table 7 – Summary results of equivalent-resistance analysis	43
	46
Table 9 – Example of voltage classification assuming for the outdoor field strength: $E_{\text{max}}$ = 60 V/m and $E_{\text{min}}$ = 0,01 V/m	47
Table 10 – Summary of the parameters used in the numerical examples presented in Figures 16 and 17	51
Table 11 – Frequencies of interest in ITU designated bands from Table 9 of CISPR 11:2009	58
Table 12 – Electrical constants for "medium dry ground" [31] (CCIR: medium dry ground; rocks; sand; medium sized towns[32])	59
Table 13 – Electrical constants for "wet ground" [31] (CCIR: marshes (fresh water); cultivated land [24]) and "very dry ground" [31] (CCIR: very dry ground; granite mountains in cold regions; industrial areas [32])	59
Table 14 – Estimates of the errors in prediction of radiation in vertical directions based on a measurement height scan from 1 m to 4 m at known distances, d; frequency = 75 MHz (adapted from [39])	67
Table 15 – Estimates of the errors in prediction of radiation in vertical directions based on a measurement height scan from 1 m to 4 m at known distances, d; frequency = 110 MHz (adapted from [39])	71
Table 16 – Estimates of the errors in prediction of radiation in vertical directions based on a measurement height scan from 1 m to 4 m at known distances, $d$ ; frequency = 243 MHz (adapted from [39])	76
Table 17 – Estimates of the errors in prediction of radiation in vertical directions based on a measurement height scan from 1 m to 4 m at known distances, d; frequency = 330 MHz (adapted from [39])	81
Table 18 – Estimates of the errors in prediction of radiation in vertical directions based on a measurement height scan from 1 m to 4 m at known distances, $d$ ; frequency = 1 000 MHz (adapted from [39])	
Table 19 – Predictability of radiation in vertical directions at 100 kHz, using ground-based measurements of horizontally oriented $H$ -field at distances up to 3 km from the source (figures are located in 4.6.8)	101
Table 20 – Predictability of radiation in vertical directions at 1 MHz, using ground-based measurements of horizontally oriented $H$ -field at distances up to 300 m from the source (figures are located in 4.6.8)	103
Table 21 – Predictability of radiation in vertical directions at 10 MHz, using ground-based measurements of horizontally oriented $H$ -field at distances up to 300 m from the source (figures are located in 4.6.8)	104
Table 22 – Predictability of radiation in vertical directions at 30 MHz, using ground-based measurements of horizontally oriented $H$ -field at distances up to 300 m from the source (figures are located in 4.6.8)	105
Table 23 – Conditions for measuring communication quality degradation	140
Table 24 – Average and rms values of noise level normalized by $N_{f 0}$	141
Table 25 – Conditions for measuring communication quality degradation of Bluetooth	143

TR CISPR 16-3 © IEC:2010(E)

**–** 13 **–** 

Table 26 – Average and rms values of noise level normalized by $N_{f 0}$ 1	144
Table 27 – Average and rms values of noise level normalized by $N_{f 0}$ 1	145
Table 28 – Conditions for measuring communication quality degradation of W-CDMA 1	147
Table 29 – Average and rms values of noise level normalized by $N_{f 0}$ 1	148
Table 30 – Conditions for measuring the PHS throughput1	150
Table 31 – Conditions for measuring the BER of PHS1	150
Table 32 – Average and rms values of noise level normalized by $\it N_0$ 1	151
Table 33 – Overview of types of interference used in the experimental study of weighting characteristics1	164
Table 34 – DRM radio stations received for the measurement of the weighting characteristics	168
Table 35 – Comparison of BER values for the same interference lever1	172
Table 36 – Transmission parameters of DVB-T systems used in various countries1	173
Table 37 – Example of measurement results in dB(μV) of unmodulated and FM modulated carriers for various detectors (bandwidth 120 kHz)	186
Table 38 – Survey of the corner frequencies found in the various measurement results 1	187
Table 39 – Measurement results for broadband disturbance sources (measurements with rms-average and quasi-peak detectors are normalized to average detector values)1	191
Table 40 – Expected deviations between different laboratories for small EUTs due to variations of the impedance $Z_{ m apparent}$ at point B1	192
Table 41 – Calibration measurement results format2	201
Table 42 – Scan times	219
Table 43 – Sampling rates for different BWIF	223
Table 44 – Scan times for a scan 30 MHz to 1 GHz	224

#### **- 14 -**

## INTERNATIONAL ELECTROTECHNICAL COMMISSION

# SPECIFICATION FOR RADIO DISTURBANCE AND IMMUNITY MEASURING APPARATUS AND METHODS –

# Part 3: CISPR technical reports

#### **FOREWORD**

- 1) The International Electrotechnical Commission (IEC) is a worldwide organization for standardization comprising all national electrotechnical committees (IEC National Committees). The object of IEC is to promote international co-operation on all questions concerning standardization in the electrical and electronic fields. To this end and in addition to other activities, IEC publishes International Standards, Technical Specifications, Technical Reports, Publicly Available Specifications (PAS) and Guides (hereafter referred to as "IEC Publication(s)"). Their preparation is entrusted to technical committees; any IEC National Committee interested in the subject dealt with may participate in this preparatory work. International, governmental and non-governmental organizations liaising with the IEC also participate in this preparation. IEC collaborates closely with the International Organization for Standardization (ISO) in accordance with conditions determined by agreement between the two organizations.
- 2) The formal decisions or agreements of IEC on technical matters express, as nearly as possible, an international consensus of opinion on the relevant subjects since each technical committee has representation from all interested IEC National Committees.
- 3) IEC Publications have the form of recommendations for international use and are accepted by IEC National Committees in that sense. While all reasonable efforts are made to ensure that the technical content of IEC Publications is accurate, IEC cannot be held responsible for the way in which they are used or for any misinterpretation by any end user.
- 4) In order to promote international uniformity, IEC National Committees undertake to apply IEC Publications transparently to the maximum extent possible in their national and regional publications. Any divergence between any IEC Publication and the corresponding national or regional publication shall be clearly indicated in the latter
- 5) IEC itself does not provide any attestation of conformity Independent certification bodies provide conformity assessment services and, in some areas, access to IEC marks of conformity. IEC is not responsible for any services carried out by independent certification bodies.
- 6) All users should ensure that they have the latest edition of this publication.
- 7) No liability shall attach to IEC or its directors, employees, servants or agents including individual experts and members of its technical committees and IEC National Committees for any personal injury, property damage or other damage of any nature whatsoever, whether direct or indirect, or for costs (including legal fees) and expenses arising out of the publication, use of, or reliance upon, this IEC Publication or any other IEC Publications.
- 8) Attention is drawn to the Normative references cited in this publication. Use of the referenced publications is indispensable for the correct application of this publication.
- 9) Attention is drawn to the possibility that some of the elements of this IEC Publication may be the subject of patent rights. IEC shall not be held responsible for identifying any or all such patent rights.

The main task of IEC technical committees is to prepare International Standards. However, a technical committee may propose the publication of a technical report when it has collected data of a different kind from that which is normally published as an International Standard, for example "state of the art."

CISPR 16-3, which is a technical report, has been prepared by CISPR subcommittee A: Radio-interference measurements and statistical methods.

This third edition of CISPR 16-3 cancels and replaces the second edition published in 2003, and its Amendments 1 (2005) and 2 (2006). It is a technical revision.

The main technical change with respect to the previous edition consist of the addition of a new clause to provide background information on FFT instrumentation.

TR CISPR 16-3 © IEC:2010(E)

**- 15 -**

The text of this technical report is based on the following documents:

Enquiry draft	Report on voting
CISPR/A/888/DTR	CISPR/A/899/RVC

Full information on the voting for the approval of this technical report can be found in the report on voting indicated in the above table.

A list of all parts of the CISPR 16 series can be found, under the general title *Specification for radio disturbance and immunity measuring apparatus and methods*, on the IEC website.

This publication has been drafted in accordance with the ISO/IEC Directives, Rart 2.

The committee has decided that the contents of this publication will remain unchanged until the stability date indicated on the IEC web site under "http://webstore.iec.ch" in the data related to the specific publication. At this date, the publication will be

- · reconfirmed,
- · withdrawn,
- · replaced by a revised edition, or
- · amended.

A bilingual version of this publication may be issued at a later date.

IMPORTANT – The 'colour inside' logo on the cover page of this publication indicates that it contains colours which are considered to be useful for the correct understanding of its contents. Users should therefore print this document using a colour printer.

#### **–** 16 **–**

# SPECIFICATION FOR RADIO DISTURBANCE AND IMMUNITY MEASURING APPARATUS AND METHODS –

# Part 3: CISPR technical reports

## 1 Scope

This part of CISPR 16 is a collection of technical reports (Clause 4) that serve as background and supporting information for the various other standards and technical reports in CISPR 16 series. In addition, background information is provided on the history of CISPR, as well as a historical reference on the measurement of interference power from household and similar appliances in the VHF range (Clause 5).

Over the years, CISPR prepared a number of recommendations and reports that have significant technical merit but were not generally available. Reports and recommendations were for some time published in CISPR 7 and CISPR 8.

At its meeting in Campinas, Brazil, in 1988, CISPR subcommittee A agreed on the table of contents of Part 3, and to publish the reports for posterity by giving the reports a permanent place in Part 3.

With the reorganization of CISPR 16 in 2003, the significance of CISPR limits material was moved to CISPR 16-4-3, whereas recommendations on statistics of disturbance complaints and on the report on the determination of limits were moved to CISPR 16-4-4. The contents of Amendment 1 (2002) of CISPR 16-3 were moved to CISPR 16-4-1.

NOTE As a consolidated collection of independent technical reports, this document may contain symbols that have differing meanings from one clause to the next. Attempts have been made to minimize this to the extent possible at the time of editing.

## 2 Normative references

The following referenced documents are indispensable for the application of this document. For dated references, only the edition cited applies. For undated references, the latest edition of the referenced document (including any amendments) applies.

CISPR 11:2009, Industrial, scientific and medical equipment – Radio-frequency disturbance characteristics – Limits and methods of measurement

CISPR 16-1-1, Specification for radio disturbance and immunity measuring apparatus and methods – Part 1-1: Radio disturbance and immunity measuring apparatus – Measuring apparatus

IEC 60050-161:1990, International Electrotechnical Vocabulary (IEV) – Chapter 161: Electromagnetic compatibility

IEC 60050-300:2001, International Electrotechnical Vocabulary (IEV) – Electrical and electronic measurements and measuring instruments – Part 311: General terms relating to measurements – Part 312: General terms relating to electrical measurements – Part 313: Types of electrical measuring instruments – Part 314: Specific terms according to the type of instrument

ISO/IEC Guide 99:2007, International vocabulary of metrology – Basic and general concepts and associated terms (VIM)